



OPEN

Enhancing the electrical properties of graphite nanoflake through gamma-ray irradiation

Anh Tuan Nguyen¹, Youlim Lee², Phuong Quang Hoang Nguyen³, Przemyslaw Dera³, Sang-Hee Yoon^{2✉} & Woochul Lee^{1✉}

Understanding changes in material properties through external stimuli is critical to validating the expected performance of materials as well as engineering material properties in a controlled manner. Here, we investigate a change in the c-axis electrical properties of graphite nanoflakes (GnFs) induced by gamma-ray irradiation, using conductive probe atomic force microscopy (CP-AFM). The fundamentals behind the change in their electrical properties are elucidated by analyzing the interlayer spacing, graphitization, and morphology. An increase in gamma-ray irradiation dose for GnFs leads to an exponential increase in the electrical conductance and a gradual decrease in the interlayer spacing, while accompanying indistinguishable changes in their morphology. Our experimental results suggest that the c-axis electrical conductance enhancement of GnFs with gamma-ray irradiation might be attributed to a reduction in interlayer spacing, though the created defects may also play a role. This study demonstrates that gamma-ray irradiation can be a promising route to tailor the electrical properties of GnFs.

Graphite nanoflake (GnF), one of the advanced carbon-based materials, possesses extraordinary properties such as low density, high temperature/water resistance, remarkable lubricity, excellent flexibility, etc.^{1,2}. Owing to its excellent properties, GnF has emerged as a promising nanofiller for functional polymer matrix composites that are widely used in sensors³, fire retardants^{4–6}, energy storage devices⁷, etc. The need for materials that can tolerate harsh environments sparked investigations of carbon-based materials⁸. Specifically, graphite⁹, graphene¹⁰, and carbon nanotubes¹¹ have been extensively studied for applications in harsh radiation environments such as a satellite and spent nuclear fuel. For gamma-ray irradiation on carbon-based materials, most of the previous efforts with carbon-based materials concentrated on high gamma radiation doses of MGy or higher, and investigated mainly changes in the internal structures (e.g., structural order, graphitization, etc.)^{12–15}. However, the effects of low gamma radiation doses of few kGy or lower on the structures and properties of carbon-based materials have rarely been reported. To the best of our knowledge, no study has been conducted on the GnF irradiated by gamma-ray and on a variation in the electrical conductance of GnF induced by gamma-ray irradiation. Recently, the versatility of GnF has led to extensive studies on polymer nanocomposites reinforced with GnF for radiation environments. For example, Kim et al. tried to monitor the structural integrity of dry storage canisters for spent nuclear fuels using GnF-based conductive polymer nanocomposites¹⁶. Although the nanocomposites are to be exposed to gamma-ray from radioactive waste, the study contains no information on the structural and property changes of GnF by gamma-ray irradiation. Here, we characterize a change in the electrical properties of the GnF caused by low-level gamma radiation doses and elucidate a primary cause of the change. Conductive probe atomic force microscopy (CP-AFM) is employed to measure the c-axis electrical conductance of a set of GnF samples exposed to different gamma radiation doses of 0.0 (no radiation) to 5.0 kGy. Next, a variety of characterization methods, including Raman spectroscopy, X-ray powder diffraction (XRD), scanning electron microscope (SEM), and transmission electron microscopy (TEM), are used to obtain the interlayer spacing, graphitization, and morphology of the GnF samples. Next, we correlate the change in electrical conductance with internal structural parameters of gamma-ray irradiated GnF to find a relation. The potential for enhancing and tailoring the electrical properties of GnF through gamma-ray irradiation is also addressed.

¹Department of Mechanical Engineering, University of Hawaii at Manoa, Honolulu, HI 96822, USA. ²Bioinspired Engineering Laboratory, Department of Mechanical Engineering, Inha University, Incheon 22212, Republic of Korea. ³Hawaii Institute of Geophysics and Planetology, University of Hawaii at Manoa, Honolulu, HI 96822, USA. ✉email: shyoon@inha.ac.kr; woochull@hawaii.edu

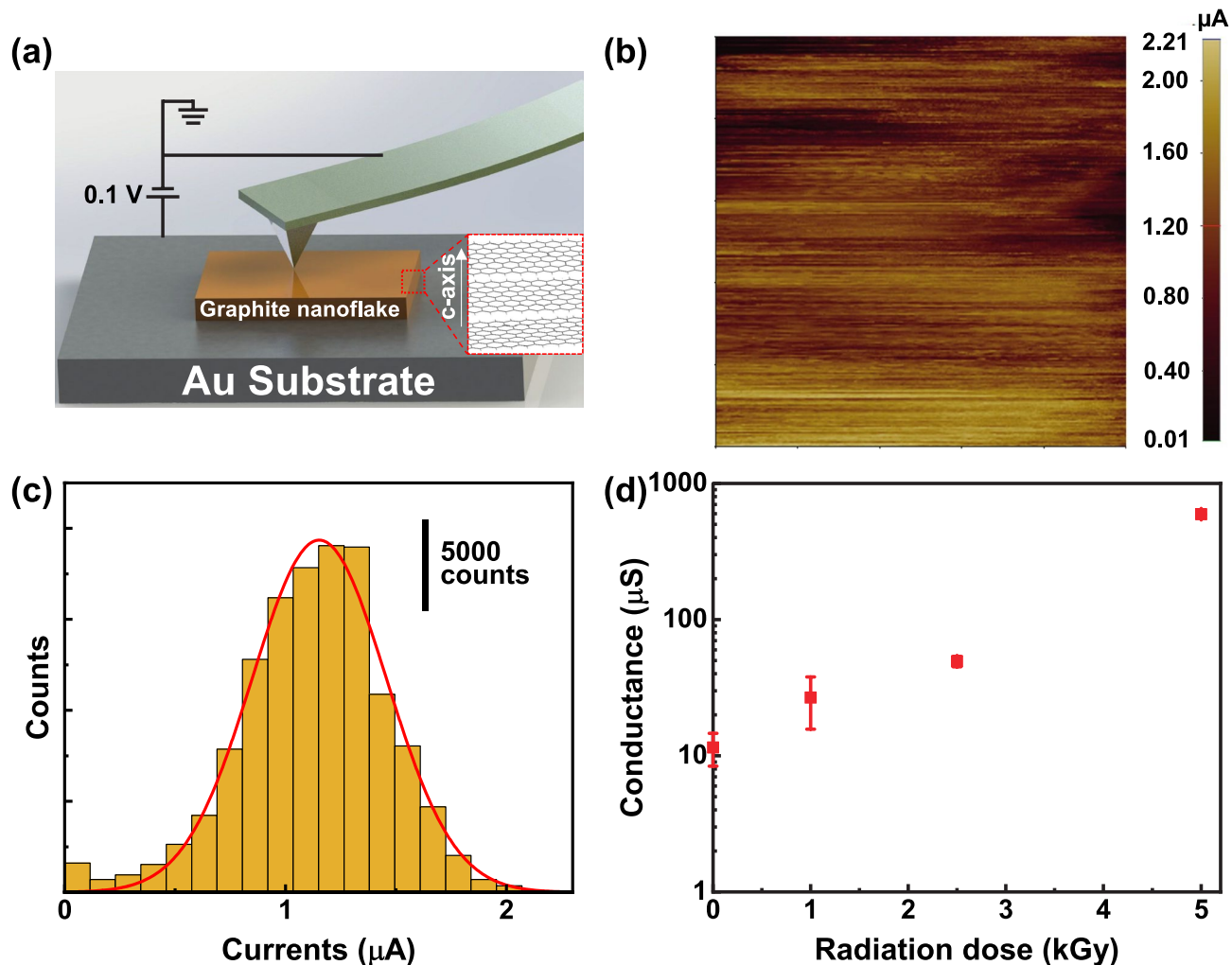


Figure 1. Electrical conductance of GnFs exposed to different gamma-ray radiation doses. (a) The schematic of CP-AFM for measuring electrical conductance. The inset in (a) shows the schematic of GnFs orientation in the measurement, the basal plane of GnFs parallel to the Au substrate. (b) 2D current map of GnF sample with no gamma-ray irradiation (i.e., 0.0 kGy). The scanning size is $250 \times 250 \text{ nm}^2$. (c) Current histogram obtained from the 0.0 kGy GnF. The current histogram is constructed from 2D current map [shown in (b)]. The value of average current is obtained by performing a curve fitting analysis to the current histogram with Gaussian distribution. (d) Electrical conductance versus gamma-ray radiation dose. An increase in gamma-ray radiation dose leads to an exponential increase in the electrical conductance of GnFs.

Materials and methods

Materials. Natural graphite was purchased from Asbury Carbons (NJ, USA). Potassium permanganate (KMnO_4) and nitric acid (HNO_3) were obtained from Sigma-Aldrich (MO, USA). All chemicals used for GnF synthesis were of reagent grade and used as received.

Preparation of GnF. GnF samples were prepared from natural graphite using the method described in our previous study¹. In brief, natural graphite was intercalated by mixing with KMnO_4 (oxidant) and HNO_3 (intercalant) at a weight ratio of 1:1:2 (graphite: KMnO_4 : HNO_3), followed by microwave irradiation at 700 W for 60 s for graphite exfoliation¹⁷. After washing off with deionized (DI) water, the exfoliated graphite in DI water was fragmented using an ultrasonicator (Q700, Qsonica (CT, USA)) at a power of 700 W, an amplitude of 80%, and a duty cycle of 50% for 6 h to prepare GnF samples. Next, the GnF samples were treated with a gamma-ray irradiator (Nordion, Canada) in which two gamma-rays with energy levels of 1.17 MeV and 1.34 MeV were produced by Co-60. Three doses (i.e., 1.0, 2.5, and 5.0 kGy) were accumulated at a dose rate of 10 kGy/h.

Measurement and characterization. The c-axis electrical conductance of GnF samples was measured with CP-AFM in the commercial AFM system (NX-10, Park Systems (Korea)), as CP-AFM has been widely used to characterize the electrical properties of various nanomaterials such as molecule junction¹⁸, protein¹⁹, nanowires²⁰, and thin film²¹. The GnF samples exposed to different gamma radiation doses were placed on Au substrate (Fig. 1a). Then, a platinum-coated probe tip with force constant of 2.8 N/m (NSC 18/Pt, MikroMasch

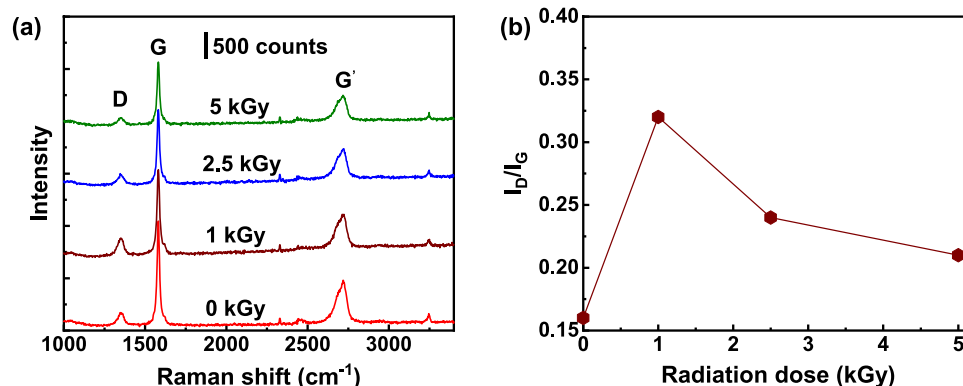


Figure 2. Raman spectroscopy analysis. (a) Raman spectra of GnF with varying gamma-ray radiation doses of 0.0, 1.0, 2.5, and 5.0 kGy. (b) I_D/I_G ratio as a function of radiation dose.

(Estonia)) was in contact with the GnF samples at a constant force of 25 nN. To measure current, a DC voltage of 0.1 V was applied to the Au substrate and ground was applied to the GnF samples. It is worth noting that we first examined I-V curves to ensure that the CP-AFM measurements are in linear ohmic regime (see Fig. S1 in supplementary material). The internal structures of GnFs were characterized by Raman and XRD spectroscopy. All Raman measurements of GnF samples were performed with the DXR2xi Raman imaging microscope (Thermo Scientific (MA, USA)) using 532 nm laser radiation at room temperature. XRD spectra were collected on a Bruker D8 Advance diffractometer (MA, USA) with CuK α source ($\lambda = 1.54060 \text{ \AA}$) operating at 40 mA and 40 kV in a para-focusing Bragg–Brentano mode. The measurement was performed with a step size of 0.02° and 4 s per step. The morphology of GnFs was characterized by SEM and TEM. For SEM, GnFs were mounted with conductive carbon tape and viewed with a Hitachi S-4800 FESEM at an accelerating voltage of 5 kV. The TEM image was captured from a Hitachi HT7700 TEM at 100 kV and photographed with an AMT XR-41B 2 k \times 2 k CCD camera.

Results and discussion

The c-axis electrical conductance of the GnF samples exposed to different gamma radiation doses of 0.0, 1.0, 2.5, and 5.0 kGy was quantified with CP-AFM (Fig. 1a). For reference, the gamma radiation doses of 1.0, 2.5, and 5.0 kGy are approximately equivalent to the accumulated gamma-ray emitted from dry storage canisters (for spent nuclear fuels) for 16, 40, and 80 years, respectively. Each GnF sample was scanned in a contact mode with a scan size of $250 \times 250 \text{ nm}^2$ to obtain its 2D current map. A representative 2D current map of pristine GnF (i.e., 0.0 kGy GnF) is shown in Fig. 1b (see Fig. S2 in supplementary material for 2D current maps of GnFs with 1.0, 2.5, and 5.0 kGy). After obtaining the current map, data analysis was performed to obtain the average current by fitting a Gaussian distribution to the current histogram, as shown in Fig. 1c. A similar statistical analysis was carried out for 1.0, 2.5, and 5.0 kGy GnFs (Fig. S2 in supplementary material). The conductance G was then calculated from $G = I/V$, where I is the average current and V is the applied voltage. Our measurements show that the GnF without irradiation exhibits the lowest conductance value (Fig. 1d). With the accumulation of radiation dose, the conductance of GnF exponentially increases and reaches the maximum at 5.0 kGy radiation dose. We note that electrical contact area varies depending on Young's modulus of samples²², which can potentially result in experiment errors. Xu et al. investigated the change of mechanical properties of carbon fiber under gamma-ray irradiation¹¹. Even though they reported that Young's modulus of carbon fiber increases with an increase of radiation dose, the change in Young's modulus is considerably small at a low dose. Thus, we neglected Young's modulus changes due to gamma-ray irradiation, and assumed the identical electrical contact area.

To understand the change in the electrical properties of GnFs caused by gamma-ray irradiation, the internal structure of the GnFs was investigated with Raman spectroscopy and XRD measurement. Raman spectroscopy is a sensitive and non-destructive technique to investigate the degree of structural perturbation in carbon-based materials^{23,24}. Figure 2a presents the Raman spectra of the GnF samples with radiation doses of 0.0, 1.0, 2.5, and 5.0 kGy. As clearly seen, two prominent peaks of graphite exist. A G-band peak (at about 1580 cm^{-1}) represents in-plane vibrations of sp^2 bonds, and a D-band peak (at about 1350 cm^{-1}) represents the structural defect and disorder associated with sp^3 hybridized carbon atoms. Another peak in the spectra is a G'-band (also called 2D band) positioned at about 2700 cm^{-1} , which corresponds to the overtone of the D-band and represents intrinsic properties of well-ordered sp^2 carbon atoms (without any kind of disorder)²⁵. I_D/I_G ratio is a useful parameter for evaluating the degree of graphitization of carbon-based materials. A higher I_D/I_G ratio indicates a smaller degree of graphitization²⁶. As the radiation dose increases, I_D/I_G value first increases from 0.0 to 1.0 kGy, and then gradually decreases afterward (Fig. 2b). This observation indicates that the graphitization first decreases and moderately increases with the radiation dose. To understand the change in graphitization, it is worth considering the different mechanisms of interaction between gamma-ray irradiation and the GnFs.

There are three interactions between gamma-ray and solid materials: photoelectron, Compton scattering, and electron pair effect²⁷. The influence of gamma-ray depends on the magnitude of gamma-quanta energy and the effective atomic number¹². The photoelectric effect happens at low energy, whereas the electron pair effect

is dominant in the high energy regime. At intermediate energy of around 1 MeV, the Compton scattering effect is the main mechanism of gamma-ray absorption. The effective atomic number of graphite can be calculated based on Mayneord equation²⁸, $Z_{\text{eff}} = (a_1 Z_1^m + a_2 Z_2^m + \dots + a_n Z_n^m)^{1/m}$, where a_1, a_2, \dots, a_n are the fractional weight of compound elements, Z_1, Z_2, \dots, Z_n are the elements atomic number, and m is an exponent indicating power dependency. For practical purposes, m is considered equal to be 2.94²⁹. For the GnFs prepared by our method, the O:C atomic ratio is 0.042 as characterized in the previous study³⁰. Then, the weight percentage of carbon and oxygen is 94.7% and 5.3%, respectively. Consequently, the effective atomic number of the GnFs can be calculated to be 6.14. The calculated effective atomic number and gamma-quanta energies of 1.17 MeV and 1.34 MeV indicate that the major interaction between gamma-ray and GnF is the Compton scattering effect¹².

The interaction between Compton scattering effect and GnFs can be described as follows. The effect of gamma-quanta energy on defect creation and annealing involves an indirect process³¹. First, the incident photon interacts with carbon atoms of graphite to produce recoil electrons and scattered photons. Then, the recoil electrons collide with graphite atomic lattice and transfer energy. When the transferred energy exceeds an atomic displacement threshold energy, it generates vacancies through sputtering³². This threshold energy of so-called knock-on damage for single-walled carbon nanotubes is roughly 86 keV³³. Gamma quanta energies used in this study are 1.17 and 1.34 MeV, which are likely sufficient to displace carbon atoms. Subsequently, the displaced atoms collide with other atoms, resulting in a collision cascade. Therefore, a large number of defects (i.e., displaced atoms) are generated and thereby disorder in structure increases. When sufficient defects are created to reach saturated level, transferred energy that is less than knock-on damage threshold energy is converted into thermal energy during the atomic collision process. As a result, local temperature increases, causing an annealing process. In this thermal annealing process, interstitial atoms diffuse and fill vacancy defects, and then crystal imperfections consequently are reduced.

Initial defect formation and subsequent crystal restoration upon gamma-ray irradiation are observed in this study. As seen in Fig. 2b, I_D/I_G ratio increases from 0.0 to 1.0 kGy, indicating defect formation in GnF. Further increasing gamma-ray irradiation results in decreasing I_D/I_G ratio, which can be attributed to the crystal restoration. We note, however, that I_D/I_G ratio of GnF with 5.0 kGy is still higher than that of GnF with 0.0 kGy, suggesting that defects are not fully restored to the level of GnF without gamma-ray irradiation exposure. Our results are consistent with previous studies^{13,32}. Cataldo used gamma-ray irradiation dose of 1 MGy with a dose rate of 5.7 kGy/h on graphite and found that the irradiated graphite presented more damage compared to the graphite without irradiation¹³. Wang et al. studied the effect of gamma-ray irradiation ranging from 0 to 3 MGy on graphene with a dose rate of 2.4 kGy/h³². They also suggested that the gamma-ray irradiation damaged graphene when the radiation dose increased from 0 to about 450 kGy, but the damage was gradually restored when the radiation dose further increased from 450 kGy to 3 MGy. They also found that the damage in graphene at 3 MGy was still greater than that in the pristine graphene. However, a study conducted by Li et al. shows results that are contradiction to those from Wang et al.'s work¹². Li et al. used gamma-ray radiation doses of 200 kGy and 2 MGy on graphite with the dose rate of 1.8 kGy/h. They found that the degree of graphitization at 200 kGy was higher than that at 2 MGy, indicating no damage restoration in higher gamma irradiation dose. This discrepancy could be caused by the dose rate differences. Wang et al. used a higher dose rate of 2.4 kGy/h. In this study, we used even higher dose rate of 10 kGy/h, and our results are in agreement with those from Wang et al.'s work. A higher dose rate generates recoil electrons more rapidly. Thus, we suggest that even at a low radiation dose (1.0 kGy), but under a high dose rate, the amount of generated recoil electron is large enough to damage the graphite, while a further increase in the radiation dose leads to damage restoration.

While Raman spectroscopy revealed the degree of structure disorder, our findings from Raman spectroscopy cannot explain the conductance change upon gamma-ray irradiation, since no direct correlations were observed. In order to further elucidate the structure–property relationship, we performed XRD characterization. In XRD characterization, adding internal reference material to the sample helps obtain accurate results, since a minor error can result from the height difference of sample³⁴. In this work, NiO was chosen as an internal reference material. The powder patterns were corrected based on the NiO referenced pattern (PDF 000–047–1049) from PDF 4+ database³⁵. The enlarged XRD spectra of a peak (002) at $2\theta \approx 26.5^\circ$ of our GnF samples with varying gamma-ray irradiation doses is shown in Fig. 3a. The full XRD spectra of GnFs and NiO can be found in Fig. S3 of the supplementary document. A closer look at the (002) peak reveals that it shifts to a higher angle with the increase of radiation dose. Based on the (002) peak position, interlayer spacing between the layers of GnFs can be calculated from the Bragg equation: $d = \frac{\lambda}{2\sin\theta}$, where d is interlayer spacing, λ is incident wavelength, and θ is the corrected Bragg angle. As the radiation dose increases from 0.0 to 5.0 kGy, the interlayer spacing of GnF monotonically decreases from 0.3359 to 0.3349 nm, as shown in Fig. 3b. Previous studies investigated the effect of gamma-ray irradiation with the range of 0 to 2 MGy on graphite^{12,36}. Their results also showed that graphite's interlayer spacing decreases as radiation dose increases. The values of 2θ , interlayer spacing, and electrical conductance of gamma-ray irradiated GnFs are tabulated in Table S1 of supplementary material along with uncertainties of 2θ and interlayer spacing obtained from the peak fit using TOPAS5. We note that GnFs investigated in this work show interlayer spacing values very close to the value of pure graphite (0.3354 nm)³⁷, indicating that graphite intrinsic structure is maintained.

The c-axis electrical conductance as a function of interlayer spacing for the gamma-ray irradiated GnFs is reported in Fig. 3c. It can be clearly seen that the conductance exponentially increases with the decrease of interlayer spacing, suggesting that the increase in electrical conductance of GnFs can be attributed to the reduced interlayer spacing. Prior studies have demonstrated a relation between interlayer spacing and electrical properties of graphite, which can support our experimental observations. Sutter et al. measured the c-axis electrical resistance of two-layer graphene while the separation between two layers was varied through different compressions with probes³⁸. Their results show that electrical resistance exponentially decreases as the separation is reduced. In addition, Kozhemyakina et al. reported interlayer spacing dependence on electrical conductivity of graphite

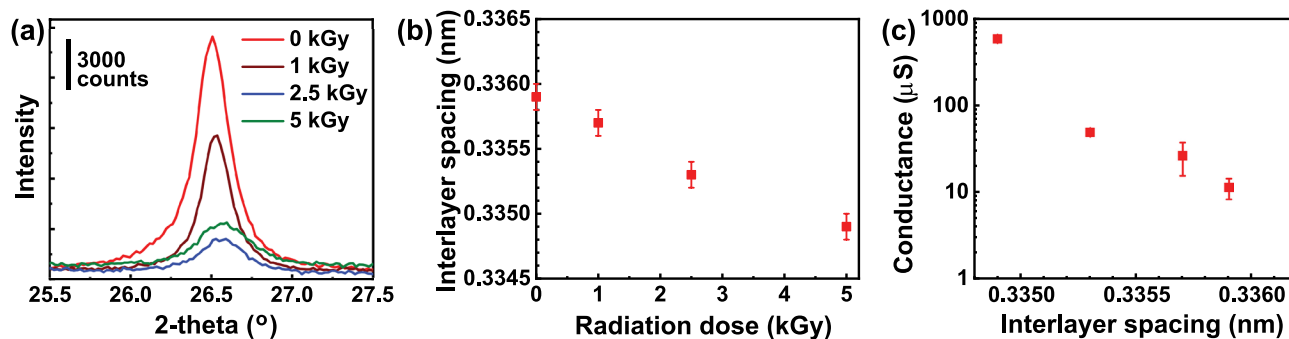


Figure 3. XRD spectroscopy analysis. (a) (002) peak of XRD spectra of GnF samples with varying gamma-ray radiation doses of 0.0, 1.0, 2.5, and 5.0 kGy. (b) Interlayer spacing of GnFs as a function of radiation dose. (c) Semi-log plot of electrical conductance as a function of interlayer spacing for GnFs. Exponential increase of conductance is observed as interlayer spacing is reduced.

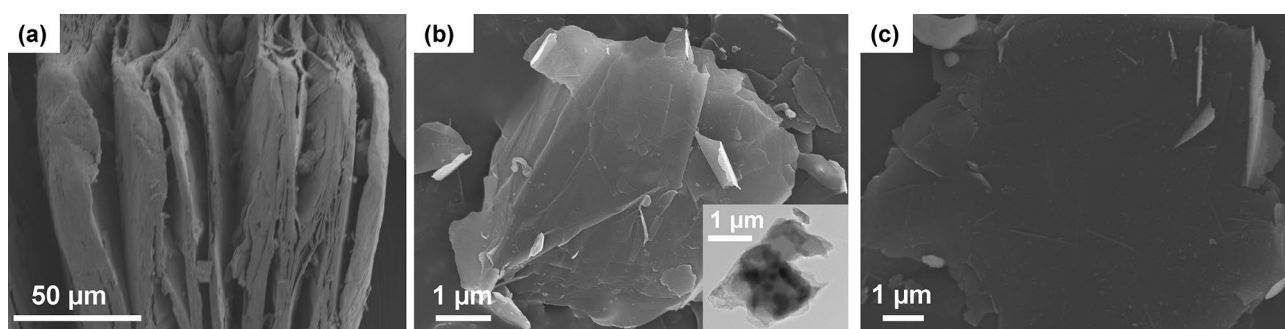


Figure 4. Characterization of GnF morphologies. (a) Intercalated graphite (before exfoliation). (b–c) GnFs with a gamma-ray radiation dose of (b) 0.0 kGy and (c) 5.0 kGy. Inset in (b) shows the TEM image.

pellets³⁹. Several grades of graphite were prepared, and their results indicate that the electrical conductivity decreases as interlayer spacing decreases. While these studies are relevant to our study, we note that more study is essential to elucidate a detailed mechanism behind the exponential dependence of electrical resistance on the interlayer spacing of gamma-ray irradiated GnFs. Several tunneling mechanisms can play a role in cross-plane charge transport of van der Waals layered materials. For example, Najmaei et al. employed a direct tunneling, Poole–Frenkel trap-based tunneling, and hopping conduction through the layers to describe out of plane charge transport in NbSe₂ and HfS₂⁴⁰. While direct tunneling depends only on the applied electric field, trap-based tunneling and hopping conduction depend on temperature in addition to the electric field. Thus, temperature dependent current–voltage measurements on GnFs can enable quantitative analysis using the barrier models to discover which transport mechanisms are dominant in gamma ray irradiated GnF samples. Further, other factors such as stacking-faults and stacking sequence (i.e., Bernal vs. rhombohedral stacking) may also play a substantial role in c-axis transport, as it starts getting demonstrated in recent studies⁴¹. We also note that although I_D/I_G ratio from Raman spectroscopy does not show a direct relation with c-axis conductance, defect density and types may play a role in c-axis charge transport, which warrants further study.

Next, we checked the morphology of GnFs to examine the alterations resulting from the gamma-ray exposure. SEM and TEM images were obtained from intercalated graphite, GnF without gamma-ray exposure, and GnF after 5.0 kGy gamma-ray exposure (Fig. 4). For the intercalated graphite, the layered structure is clearly visible, as shown in Fig. 4a. SEM image is obtained for GnFs without gamma-ray irradiation (Fig. 4b). Figure 4c presents GnFs after 5.0 kGy gamma-ray irradiation. A comparison of the surface morphology between GnFs without gamma-ray irradiation and after 5.0 kGy radiation exposure reveals indistinguishable changes, suggesting that the gamma-ray irradiation up to 5.0 kGy does not induce notable changes on GnF surface. However, we note that the morphology of carbon-based materials could be changed if a higher radiation dose (order of 100 kGy) is applied as demonstrated in the previous work⁴².

Conclusions

We enhanced the c-axis electrical conductance of small stacks of graphene (i.e., GnFs) through gamma-ray irradiation. The degree of enhancement in the electrical conductance was quantified with CP-AFM. Subsequently, internal structure and morphology (i.e., interlayer spacing, graphitization, and morphology) were investigated with XRD, Raman spectroscopy, and SEM/TEM to find a relation between electrical property and structures. Change in low gamma radiation doses from 0.0 to 5.0 kGy leads to an exponential increase in the electrical conductance of GnFs. An increase in gamma-ray radiation results in a monotonic decrease in the interlayer

spacing of GnFs, but their morphology change is unnoticeable. The experimental characterization suggests that the enhancement of *c*-axis electrical conductance of GnF might be attributed to a reduction of the interlayer spacing. Raman spectroscopy measurements indicate that knock-on damage occurs at 1.0 kGy, and graphitization is somewhat restored from 2.5 to 5.0 kGy, but not the extent of pristine GnFs (i.e., GnFs with no gamma-ray exposure). Our findings provide valuable insight into changes in the electrical properties and internal structures of GnFs under low gamma-ray radiation doses. In addition, this work will have significant implications for tailoring material properties of GnFs and other carbon-based materials.

Data availability

The data presented in this study are available on request from the corresponding authors.

Received: 1 June 2022; Accepted: 25 August 2022

Published online: 01 September 2022

References

- Park, S., Kim, J., Jeon, K.-J. & Yoon, S.-H. Characterization on the Expanding nature of graphite in microwave-irradiated exfoliation. *J. Nanosci. Nanotechnol.* **16**, 4450–4455 (2016).
- Chung, D. D. L. Exfoliation of graphite. *J. Mater. Sci.* **22**, 4190–4198 (1987).
- Kim, J., Oh, S. & Yoon, S.-H. Parameter study of microwave assisted exfoliation of graphite and its application to large deformation strain sensors, in *IEEE SENSORS 2014 Proceedings* 1699–1702 (IEEE, 2014). <https://doi.org/10.1109/ICSENS.2014.6985349>
- Modesti, M., Lorenzetti, A., Simioni, F. & Camino, G. Expandable graphite as an intumescent flame retardant in polyisocyanurate-polyurethane foams. *Polym. Degrad. Stab.* **77**, 195–202 (2002).
- Duquesne, S. *et al.* Expandable graphite: A fire retardant additive for polyurethane coatings. *Fire Mater.* **27**, 103–117 (2003).
- Wang, Z., Han, E. & Ke, W. Influence of expandable graphite on fire resistance and water resistance of flame-retardant coatings. *Corros. Sci.* **49**, 2237–2253 (2007).
- Wu, Y. *et al.* Synthesis of few-layer N-doped graphene from expandable graphite with melamine and its application in supercapacitors. *Chin. Chem. Lett.* **31**, 559–564 (2020).
- Romanosky, R. R. & Maley, S. M. Harsh environment sensor development for advanced energy systems. In *Proceedings on SPIE 8725, Micro- and Nanotechnology Sensors, Systems, and Applications V, 87250H* (eds George, T. *et al.*) (2013). <https://doi.org/10.1117/12.2015865>.
- Hulman, M., Skákalová, V., Roth, S. & Kuzmany, H. Raman spectroscopy of single-wall carbon nanotubes and graphite irradiated by γ rays. *J. Appl. Phys.* **98**, 024311 (2005).
- Chen, L. *et al.* A facile strategy to prepare functionalized graphene via intercalation, grafting and self-exfoliation of graphite oxide. *J. Mater. Chem.* **22**, 13460–13463 (2012).
- Xu, Z., Huang, Y., Min, C., Chen, L. & Chen, L. Effect of γ -ray radiation on the polyacrylonitrile based carbon fibers. *Radiat. Phys. Chem.* **79**, 839–843 (2010).
- Li, B. *et al.* The effect of gamma ray irradiation on the structure of graphite and multi-walled carbon nanotubes. *Carbon* **60**, 186–192 (2013).
- Cataldo, F. A Raman study on radiation-damaged graphite by γ -rays. *Carbon* **38**, 634–636 (2000).
- Galván, D. H., Garzón, I. L., Santiago, P. & José-Yacamán, M. Structural changes and electronic properties of gamma irradiated graphite: An experimental and theoretical study. *Fuller. Sci. Technol.* **6**, 867–883 (1998).
- Ansón-Casaos, A. *et al.* The effect of gamma-irradiation on few-layered graphene materials. *Appl. Surf. Sci.* **301**, 264–272 (2014).
- Kim, Y., Kim, T., Chung, S. & Yoon, S.-H. Development of smart material-based structural integrity monitoring sensors for detecting the fracture sign in dry storage, in *Topfuel* (2018).
- Park, S. *et al.* Mechano-electrical properties of a GnF/PDMS composite controlled by the aspect ratio and concentration of GnF. *Compos. Sci. Technol.* **159**, 77–86 (2018).
- Wold, D. J. & Frisbie, C. D. Fabrication and characterization of metal–molecule–metal junctions by conducting probe atomic force microscopy. *J. Am. Chem. Soc.* **123**, 5549–5556 (2001).
- Li, W. *et al.* Temperature and force dependence of nanoscale electron transport via the Cu protein azurin. *ACS Nano* **6**, 10816–10824 (2012).
- Alvarez, J. *et al.* Conductive-probe atomic force microscopy characterization of silicon nanowire. *Nanoscale Res. Lett.* **6**, 110 (2011).
- Kleider, J. P., Longeaud, C., Brüggemann, R. & Houzé, F. Electronic and topographic properties of amorphous and microcrystalline silicon thin films. *Thin Solid Films* **383**, 57–60 (2001).
- Liu, S. & Wang, Q. J. Determination of Young's modulus and Poisson's ratio for coatings. *Surf. Coat. Technol.* **201**, 6470–6477 (2007).
- Dresselhaus, M. S., Jorio, A. & Saito, R. Characterizing graphene, graphite, and carbon nanotubes by Raman spectroscopy. *Annu. Rev. Condens. Matter Phys.* **1**, 89–108 (2010).
- Ferrari, A. C. Raman spectroscopy of graphene and graphite: Disorder, electron–phonon coupling, doping and nonadiabatic effects. *Solid State Commun.* **143**, 47–57 (2007).
- Pimenta, M. A. *et al.* Studying disorder in graphite-based systems by Raman spectroscopy. *Phys. Chem. Chem. Phys.* **9**, 1276–1290 (2007).
- Vanitha, M., Camellia, P. & Balasubramanian, N. Augmentation of graphite purity from mineral resources and enhancing % graphitization using microwave irradiation: XRD and Raman studies. *Diam. Relat. Mater.* **88**, 129–136 (2018).
- Xu, Z. *et al.* Nano-structure and property transformations of carbon systems under γ -ray irradiation: A review. *RSC Adv.* **3**, 10579 (2013).
- Khan, F. M. & Gibbons, J. P. *Khan's the Physics of Radiation Therapy* (Lippincott Williams & Wilkins, 2014).
- Nawi, S. N. M. *et al.* Polymer pencil lead graphite for in vivo radiation dosimetry. *Diam. Relat. Mater.* **106**, 107860 (2020).
- Ha, S., Choi, Y., Lee, W., Kim, Y. & Yoon, S.-H. Prediction of mechanical properties of graphite nanoflake/polydimethylsiloxane nanocomposites as affected by processing method. *Compos. B Eng.* **224**, 109186 (2021).
- Nikolaenko, V. A. & Karpukhin, V. I. Radiation annealing of defects under the effect of γ -radiation. *J. Nucl. Mater.* **233**, 1067–1069 (1996).
- Wang, Y. *et al.* Influence of irradiation upon few-layered graphene using electron-beams and gamma-rays. *Appl. Phys. Lett.* **105**, 023102 (2014).
- Smith, B. W. & Luzzi, D. E. Electron irradiation effects in single wall carbon nanotubes. *J. Appl. Phys.* **90**, 3509–3515 (2001).
- Holder, C. F. & Schaak, R. E. Tutorial on powder X-ray diffraction for characterizing nanoscale materials. *ACS Nano* **13**, 7359–7365 (2019).
- Gates-Rector, S. & Blanton, T. The powder diffraction file: A quality materials characterization database. *Powder Diffr.* **34**, 352–360 (2019).
- Xu, Z. *et al.* Graphitization of polyacrylonitrile carbon fibers and graphite irradiated by γ rays. *Mater. Lett.* **63**, 1814–1816 (2009).

37. Yoon, M., Howe, J., Tibbetts, G., Eres, G. & Zhang, Z. Polygonization and anomalous graphene interlayer spacing of multi-walled carbon nanofibers. *Phys. Rev. B* **75**, 165402 (2007).
38. Sutter, P. W., Flege, J.-I. & Sutter, E. A. Epitaxial graphene on ruthenium. *Nat. Mater.* **7**, 406–411 (2008).
39. Kozhemyakina, N. V. *et al.* Effect of the structure and morphology of natural, synthetic and post-processed graphites on their dispersibility and electronic properties. *Fuller. Nanotubes Carbon Nanostruct.* **21**, 804–823 (2013).
40. Najmaei, S. *et al.* Cross-plane carrier transport in Van Der Waals layered materials. *Small* **14**, 1703808 (2018).
41. Ariskina, R. *et al.* Influence of surface band bending on a narrow band gap semiconductor: Tunneling atomic force studies of graphite with Bernal and rhombohedral stacking orders. *Phys. Rev. Mater.* **5**, 044601 (2021).
42. Xu, Z. *et al.* Effect of γ -ray irradiation grafting on the carbon fibers and interfacial adhesion of epoxy composites. *Compos. Sci. Technol.* **67**, 3261–3270 (2007).

Acknowledgements

W.L. acknowledges support from the College of Engineering at the University of Hawaii at Manoa. We thank Hawaii Corrosion Laboratory for help with Raman spectroscopy. We thank Dr. Suman Chhetri for helpful discussions and manuscript review. This research was supported by Basic Science Research Program through the National Research Foundation of Korea (NRF) funded by the Ministry of Science and ICT (2017R1A2B4010300).

Author contributions

W.L. and S.Y. conceived this work. A.T.N. conducted AFM experiments and data analysis. Y.L. prepared GnF samples. P.Q.H.N. and P.D. performed XRD characterization and data analysis. A.T.N. wrote the manuscript draft with inputs from W.L. and S.Y. W.L. and S.Y. supervised the project. All authors discussed the results, commented on the manuscript, and approved the final manuscript.

Competing interests

The authors declare no competing interests.

Additional information

Supplementary Information The online version contains supplementary material available at <https://doi.org/10.1038/s41598-022-19232-2>.

Correspondence and requests for materials should be addressed to S.-H.Y. or W.L.

Reprints and permissions information is available at www.nature.com/reprints.

Publisher's note Springer Nature remains neutral with regard to jurisdictional claims in published maps and institutional affiliations.



Open Access This article is licensed under a Creative Commons Attribution 4.0 International License, which permits use, sharing, adaptation, distribution and reproduction in any medium or format, as long as you give appropriate credit to the original author(s) and the source, provide a link to the Creative Commons licence, and indicate if changes were made. The images or other third party material in this article are included in the article's Creative Commons licence, unless indicated otherwise in a credit line to the material. If material is not included in the article's Creative Commons licence and your intended use is not permitted by statutory regulation or exceeds the permitted use, you will need to obtain permission directly from the copyright holder. To view a copy of this licence, visit <http://creativecommons.org/licenses/by/4.0/>.

© The Author(s) 2022